Editors' Suggestion

Subradiance and superradiance-to-subradiance transition in dilute atomic clouds

Diptaranjan Das, B. Lemberger, and D. D. Yavuz
Department of Physics, 1150 University Avenue, University of Wisconsin at Madison, Madison, Wisconsin 53706, USA

(Received 24 January 2020; accepted 21 September 2020; published 14 October 2020)

We experimentally study subradiance in a dilute cloud of ultracold rubidium (Rb) atoms where $n\lambda_a^3 \approx 10^{-2}$ (n: atomic density; λ_a: excitation wavelength) and the on-resonance optical depth of the cloud is of order unity. We show that, in the strong excitation regime, the subradiant time scales depend on the excitation fraction of the cloud; i.e., to the intensity of the excitation pulse. In this regime, the decay dynamics are highly complicated and there is not a single decay time constant. Instead, the decay time constant varies during the dynamics. Specifically, we were able to observe signatures of superradiant-to-subradiant transition; i.e., initially the decay rate is faster than independent decay (superradiant emission), while at later times it transitions to slower (subradiant emission). We also discuss a theoretical model whose numerical results are in good agreement with the experiments.

DOI: 10.1103/PhysRevA.102.043708

I. INTRODUCTION

Since the seminal paper by Dicke [1], collective decay (superradiant or subradiant) of an ensemble of radiators has been studied by many authors and this problem continues to be relevant for a wide range of physical systems [2–5]. Much of the physics of collective decay can be understood from a classical viewpoint. If the radiation from the individual emitters interfere constructively, then the total radiated power is coherently enhanced, resulting in a decay rate larger than the independent decay rate of the individual emitters. For example, if N emitters are localized to a spatial region much smaller than the wavelength of radiation, their emissions can all be in phase, producing a decay rate $\sim N$ times faster than independent decay, $\sim N\Gamma_a$. This is the well-known Dicke limit of superradiance and has been extensively analyzed both theoretically and experimentally [2]. In contrast, if the individual radiators are antiphased appropriately, their radiation can interfere destructively, producing a decay rate slower than the independent rate (subradiance). In the Dicke limit, a simple approach to achieve subradiance would be to group the atoms in pairs, where atoms in each pair oscillate exactly out of phase.

While superradiance was first experimentally observed more than four decades ago [6,7], subradiance in an ensemble of atoms was experimentally demonstrated only very recently [8]. The reason for this is that, to observe subradiance, appropriate out-of-phase superpositions of the emitters need to be maintained for time scales that are long compared to the independent decay time. As a result, the subradiant states are fragile and are quite susceptible to dephasing. To overcome this challenge, recent observation of subradiance utilized ultracold atomic clouds at low temperatures, thereby avoiding motional dephasing. We also note that collective effects are most pronounced when there are a large number of emitters within a wavelength cube of volume; i.e., in the Dicke limit as discussed above. However, collective effects remain and can be quite important well outside this limit, even when the average spacing between the emitters is larger than the wavelength. In fact, as pointed out in Ref. [8], it is easier to observe subradiance outside the Dicke limit, since van der Waals dephasing due to short-range interactions is avoided [2].

Recent observation of subradiance used a large ultracold cloud with a very high on-resonance optical depth [8]—an optical depth (OD) of 40 or higher. As a result, the interpretation of the data is complicated by the fact that radiation trapping also plays an important role [9]. Furthermore, subradiance was observed in the weak excitation limit, where single atom excited subspace (which is of dimension N) is a reasonable approximation to the dynamics of the full Hilbert space. In this paper, we extend these pioneering results to the strong excitation regime and also to much more dilute ultracold clouds with an on-resonance OD of order unity. We show that, in this regime, the subradiant time scales depend on the excitation fraction of the cloud, which is determined by the intensity of the excitation pulse. We find that in this regime the decay dynamics are highly complicated and there is not a single decay time constant. Instead, the decay time constant varies during the dynamics. Specifically we were able to observe signatures of superradiant-to-subradiant transition. At early times of the evolution the decay rate is faster than independent decay (superradiant emission), while at later times it transitions to a slower rate (subradiant emission).

The collective decay problem from large samples in the strong-field excitation regime is notoriously quite difficult, since the dimension of the Hilbert space is 2^N, and there are no obvious symmetries that can be utilized to simplify the problem. There are very limited analytical and numerical tools that can be utilized in this regime [2]. We discuss a theoretical formalism that produces numerical results which are in good agreement with our experimental observations.

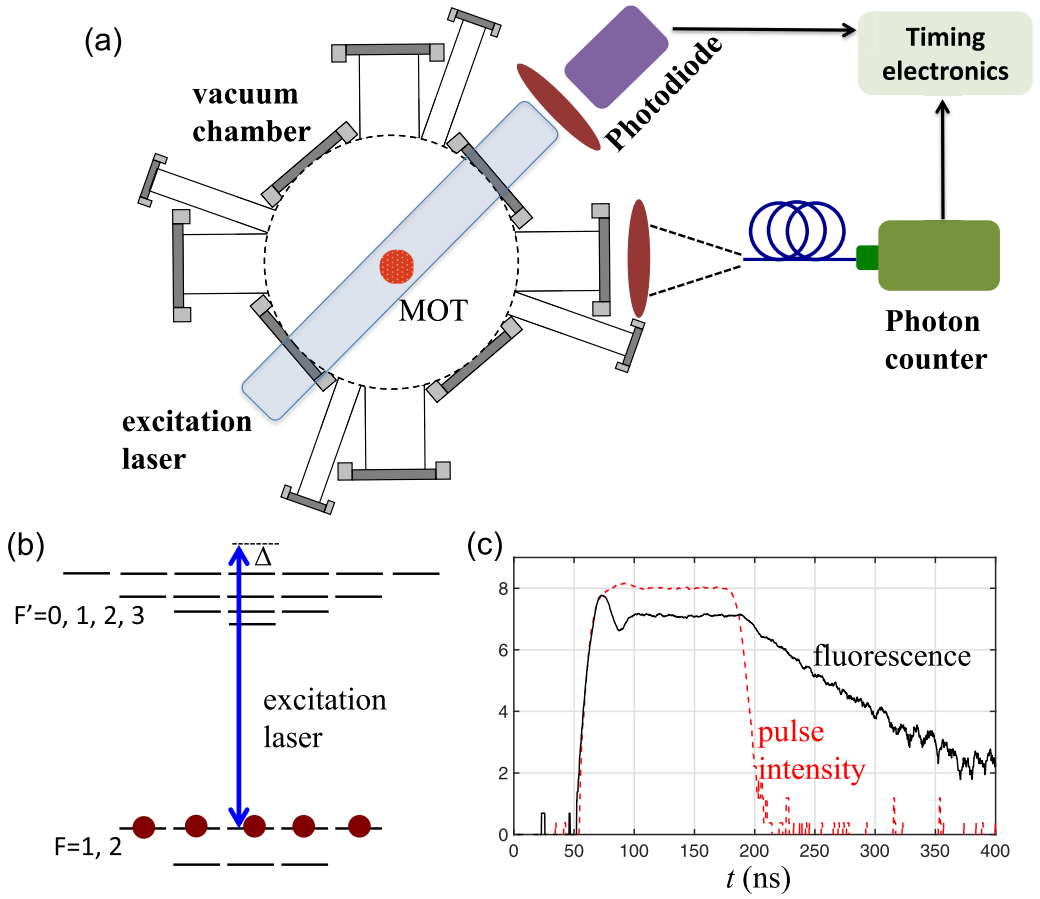

FIG. 1. (a) Simplified experimental schematic. The experiment is performed inside a 14-port stainless-steel ultrahigh vacuum chamber. We first load the ^{87}Rb atoms into a MOT from a background vapor. After the MOT is loaded and with the atoms optically pumped into the $F = 2$ ground level, the atoms are excited into $F' = 3$ level using a short and intense excitation laser. The fluorescence from the cloud is detected using a photon counter. (b) The relevant energy-level diagram of ^{87}Rb. (c) A sample fluorescence trace (solid black line) overlapped with an excitation pulse intensity trace (dashed red line), both plotted on logarithmic scale.

The formalism is motivated by the recently discovered full eigenvalue spectrum of the exchange Hamiltonian, which is an effective description of the fundamental interaction resulting in collective decay: the exchange of a photon [10].

In other important prior work, collective decay effects have been studied experimentally in a wide range of physical systems such as cold molecules [11], a system of two trapped ions [12], on multilevel transitions in hot gallium atoms [13], in cold atoms at the vicinity of a single mode nanofiber [14], and in planar metamaterial arrays [15]. Subradiant atomic momentum states were recently observed in a Bose-Einstein condensate (BEC) [16]. Studies of superradiant emission have been carried out in cold atoms in the weak excitation limit [8,17,18] as well as in diamond nanocrystals [19] and hybrid solid-state devices [20], where it is possible to study the system in the Dicke limit. Recently, switching between superradiant and subradiant states was demonstrated in a 10-qubit superconducting circuit [21]. With regard to recent theoretical work, most of these studies have focused on the weak excitation limit where a macroscopic two level atomic ensemble absorbs a single photon [22–36]. Even though this restricts the problem to a small subspace of the total Hilbert space there are several interesting effects that can be explored, for example, directional emission [22,23], photon localization [24], and collective Lamb shift [25,26]. With subradiant states being analogous to decoherence free subspaces, exploitation of subradiant states and tuning between superradiant and subradiant states can have applications in quantum memory devices and quantum information processing [37,38]. This has inspired a lot of work in studying subradiance in artificial structures like atomic arrays and with modified environments as in a cavity [39–49]. Other studies of cooperative emission include an analysis by the "Polarium model" [50], a study of spatial profile of subradiance [51], emission characteristics of entangled sources [52], and a recent analysis of many atom emission by renormalized perturbation theory [53].

II. EXPERIMENTAL SCHEMATIC

We perform our experiments inside a 14-port stainless-steel ultrahigh vacuum chamber which is kept at a base pressure 5×10^{-9} torr. A top view of our chamber is shown in Fig. 1(a). We start the experiment by cooling and loading the atoms into a magneto-optical trap (MOT). To construct the ^{87}Rb MOT, we use three counterpropagating beam pairs that are locked to the cycling $F = 2 \rightarrow F' = 3$ transition in the D2 line (transition wavelength of $\lambda_a = 780$ nm), each with a beam power of about 50 mW and a beam size of 3 cm. The

MOT lasers are obtained from a custom-built external-cavity diode laser (ECDL) whose output is amplified by semiconductor tapered amplifiers. Further details regarding our laser system can be found in our recent publications [54–56]. The MOT lasers are overlapped with a hyperfine repumping beam, which is obtained from a separate ECDL locked to the $F = 2 \rightarrow F' = 2$ transition, with an optical power of about 1 mW.

We load the atoms to the MOT from the background vapor for about 400 ms. In the last 40 ms of loading, we detune the MOT lasers to about $8\Gamma_a$ ($\Gamma_a = 2\pi \times 6.02$ MHz is the decay rate of the transition) from the cycling transition and reduce their intensity by about an order of magnitude to achieve efficient sub-Doppler cooling. At the end of the MOT loading cycle, we typically trap ∼1.3 million atoms, within a $1/e^2$ density radius of $R = 0.37$ mm, giving an on-resonance OD of $\mathrm{OD} = 3N/(\kappa_a R)^2 \sim 1$ ($\kappa_a = 2\pi/\lambda_a$ is the wave number at the transition wavelength). The atomic temperature is about 44 μK, which is measured by monitoring the free expansion of the cloud using an electron-multiplying CCD (EMCCD) camera. During the final 10 ms of the MOT loading cycle, we turn off the hyperfine repumper beam. As a result, the atoms are optically pumped into the $F = 2$ ground level at the end of the cycle.

The relevant energy-level diagram of ^{87}Rb is shown in Fig. 1(b). With the atoms optically pumped into the $F = 2$ hyperfine ground level, we turn off the MOT beams and turn on a single short and intense laser that couples the atoms to the $F' = 3$ excited level. This laser is termed the excitation laser and its duration is about 120 ns. The excitation beam is spatially larger than the size of the MOT, with a $1/e^2$ intensity radius of 0.7 mm. The highest optical power that we use in the excitation beam is ∼0.12 mW. With the atoms excited into the $F' = 3$ level, we turn off the excitation beam abruptly and record the fluorescence from the atoms using a single-photon counting module. The fast switching of the excitation beam is achieved using an acousto-optic modulator (AOM). The 90%–10% turn-off time of the excitation laser is 8 ns. We accomplish such fast switching by careful adjustment of the beam size inside the AOM.

For each photon detected, the photon counter produces an ∼10-ns-long electronic TTL pulse, which is then measured by a fast-sampling digital oscilloscope. To avoid saturation of the photon counter, we limit the number of detected photons for each experimental cycle to mostly around a photon. As a result, the experimental cycle (MOT loading-optical pumping-excitation-fluorescence detection) needs to be repeated many times to obtain a trace with a good signal-to-noise ratio. We typically repeat the experimental cycle ∼20 000 times to obtain a fluorescence trace. With each experimental cycle lasting for about 1 s, a fluorescence trace takes about 6 h to record in the laboratory. A sample fluorescence trace overlapped with an excitation pulse intensity (both on a logarithmic scale) is shown in Fig. 1(c).

III. EXPERIMENTAL DATA ANALYSIS

The excitation pulse is detected on a fast photodiode with a bandwidth of 150 MHz after the chamber. We start the data analysis after the excitation pulse has been turned off; $t = 0$ is defined to be the point where the pulse intensity has dropped to less than 10% of its peak intensity. The pulse intensity detected on the photodiode typically becomes indistinguishable from background within five nanoseconds after this point.

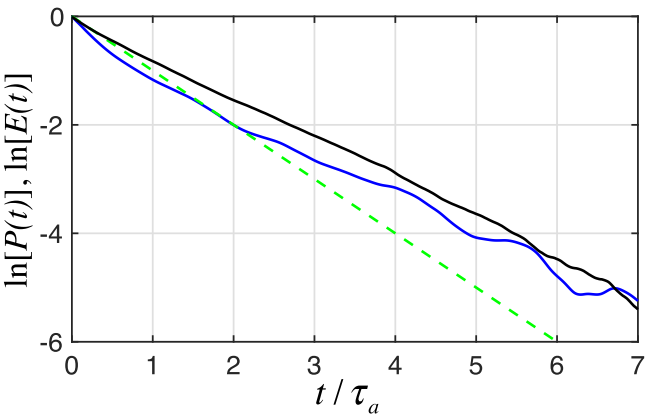

FIG. 2. Observed fluorescence $P(t)$ (solid blue line) and the inferred stored energy in the cloud $E(t) = E_0 - \int_0^t P(t')dt'$ (solid black line) as a function of time for a sample data set. Both quantities are appropriately normalized and their natural logarithms are plotted (see text for details). For comparison, the case of independent decay, $\exp(-t/\tau_a)$, is also plotted (dashed green line).

The fluorescence signal, which is recorded using the photon counter, is proportional to the optical power emitted from the cloud, and we denote this signal by $P(t)$. Most collective-decay analysis, including Dicke's original paper, focuses on the total amount of excitation in the ensemble (i.e., the population of the excited level), which is proportional to the energy stored in the cloud. We denote this quantity by $E(t)$, which is related to the emitted power through the relation $E(t) = E_0 - \int_0^t P(t')dt'$ [the inverse relationship is $P(t) = -dE(t)/dt$]. Here, E_0 is the initial (at $t = 0$) energy stored in the atomic cloud. Below, we will be plotting normalized versions of these quantities, redefined as $P(t) \equiv P(t)/P(t = 0)$ and $E(t) \equiv E(t)/E(t = 0)$. For independent decay, there is no difference between the time evolution of these two quantities since they have identical time dynamics: $E(t) \sim P(t) \sim \exp(-t/\tau_a)$ (τ_a is the lifetime of the excited level $\tau_a = 1/\Gamma_a = 26.2$ ns).

Although the photon counter detects $P(t)$, we find instead that working with $E(t)$ is more convenient for most of the data discussed below. This is because $E(t)$ involves integration over the photon counter signal, which effectively amounts to averaging and reduces the noise. An example of this is shown in Fig. 2, where we plot the natural logarithm of both of these quantities as a function of time, $\ln[P(t)]$ (solid blue line) and $\ln[(E(t)]$ (solid black line), for a sample data set. For comparison, the case of independent decay $\exp(-t/\tau_a)$ is also plotted (dashed green line). The reduced noise in $\ln[(E(t)]$ can be clearly seen in the plots. Furthermore, the two curves do not lie on top of each other, which clearly shows that the decay is not a simple exponential decay and cannot be described by a single decay time constant. As we discuss below, consistent with the theoretical model and the numerical results, the variation of the decay time constant during time evolution is better pronounced for $\ln[P(t)]$. The observed subradiance is quite remarkable considering that there are less than 10^{-2} atoms in a

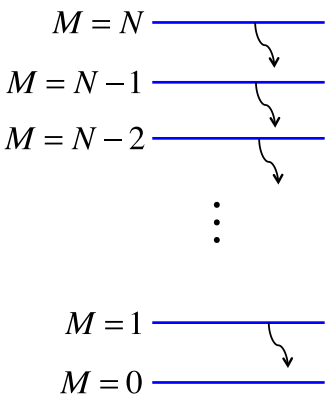

FIG. 3. Excitation decay ladder for the formalism. Each subspace with M atoms excited decays to a subspace below (i.e., $M-1$ atoms excited).

cubic wavelength of volume (i.e., $n\lambda_a^3 \approx 10^{-2}$) and the optical depth of the cloud is only of order unity. As we discuss below, the observed subradiance is consistent with the predictions of the theoretical model.

IV. THEORETICAL MODEL AND NUMERICAL SIMULATIONS

Superradiance and subradiance is well known to be quite difficult to analyze in the large sample and the strong excitation limit [2]. In the Dicke limit, with all the atoms starting in the excited level, the system can be hypothesized to remain only in symmetric superpositions [1]. This only leads to superradiance since symmetric superpositions are the states where the radiation from the emitters interfere constructively. For a large sample there are no obvious symmetries that can be employed and it is not clear how the exponentially large dimension of the Hilbert space can be simplified. Yet another complication is that, for a sample which is spatially large compared to the wavelength, the phase of the emitted radiation varies between different emitters.

To model collective decay in the large sample and strong excitation regime, we extend the excitation ladder approach as discussed in Ref. [2]. The details of our formalism will be presented in the Appendix below, but we summarize the essential ideas here. It is well known that the excitation ladder approach quantitatively captures many aspects of Dicke superradiance [2]. The key difficulty is how to extend this model for the large sample regime. For this purpose, we use a model that is motivated by the recently discovered eigenvalue spectrum of the exchange Hamiltonian, which is the basic physical interaction that causes correlated decay [10].

We consider N initially excited atoms uniformly distributed in a spherical cloud with a radius of R. The number of initially excited atoms is obtained by multiplying the total number of atoms with the excitation fraction. We split the Hilbert space into subspaces that are indexed by $M = 0, 1, \ldots, N$, which is the number of atoms in the excited state (while the remaining $N-M$ atoms are in the ground state). We denote the probability that the system is in M atom excited subspace as $\rho_M(t)$. As shown in Fig. 3, each subspace M decays to a subspace below (i.e., $M-1$ atoms excited). At $t=0$, the system starts in the $M=N$ subspace (i.e., at the top of the ladder), and then as time evolves decays down the ladder. We then have a coupled system of $N+1$ differential equations that describes the evolution of the system:

$$\frac{d\rho_M}{dt} = -\Gamma_M \rho_M + \Gamma_{M+1}\rho_{M+1}, \tag{1}$$

where the quantity Γ_M is the decay rate of subspace M to subspace $M-1$. For independent (i.e., uncorrelated) decay, $\Gamma_M = M\Gamma_a$, since for independent decay the system wave function is a product of single-atom wave functions. The key idea of our formalism is that we modify this decay rate by a quantity which is proportional to the eigenvalue distribution of the exchange Hamiltonian for each subspace, with stimulated emission heuristically incorporated. Specifically, we take

$$\Gamma_M = M\Gamma_a + \xi \frac{\sqrt{\pi + 29/12}}{k_a R}\sqrt{N-M}M\tilde{u}\Gamma_a, \tag{2}$$

where $\tilde{u}$ is a random variable whose value is uniformly distributed between $[-1, 1]$. As shown in the Appendix, Eq. (2) can be derived from our physical model with $\xi = 1$. We use the dimensionless quantity ξ as a free fitting parameter in the model, which can be viewed as the *shape* factor. This fitting parameter can be thought to account for (i) the deviation of the shape of the cloud from spherical, (ii) the uncertainty in the optical depth and, therefore, the atom number measurement of the cloud, and (iii) the uncertainty in the excitation fraction. As we discuss below, with this fitting parameter, this model successfully produces many aspects of our experimental results. In all the below fits, ξ is of order unity and varies between 0.7 and 1.

Because the sign of the random variable $\tilde{u}$ can be positive or negative, each rate Γ_M can be faster or slower than the independent decay case. For each simulation, we pick values for Γ_M as given by Eq. (2). With these values, we then numerically solve the $N+1$ coupled differential equations as given by Eq. (1) using the fourth-order Runge-Kutta method, with the system starting at the top of the ladder [i.e., with the initial condition $\rho_N(t=0) = 1$ and $\rho_M(t=0) = 0$ for all $M \neq N$]. For each simulation, we calculate the total energy stored in the cloud using $E(t) = \hbar\omega_a \sum_M M\rho_M(t)$. The radiated power is calculated using $P(t) = -dE(t)/dt$. To get an accurate description of the dynamics, we repeat the numerical simulation $\sim$1000 times, picking different values for Γ_M using Eq. (2). We obtain the final result by averaging over these simulations.

Figure 4 shows numerical results for our nominal experimental conditions: $N = 0.65$ million initially excited atoms (1.3 million atoms with an excitation fraction of 0.5) and a cloud radius of $R = 0.37$ mm. Here we plot the stored energy $E(t)$ (solid black) and radiated power $P(t)$ (solid red), both in logarithmic scale, as a function of time. Comparing Fig. 4 to the experimental traces of Fig. 2, the model reasonably captures the overall subradiance, as well as the variation in the decay time scales. However, the model overestimates the change in the decay time scales as the system evolves. One reason for this could be various dephasing mechanisms in the experiment, which is not accounted for in the model.

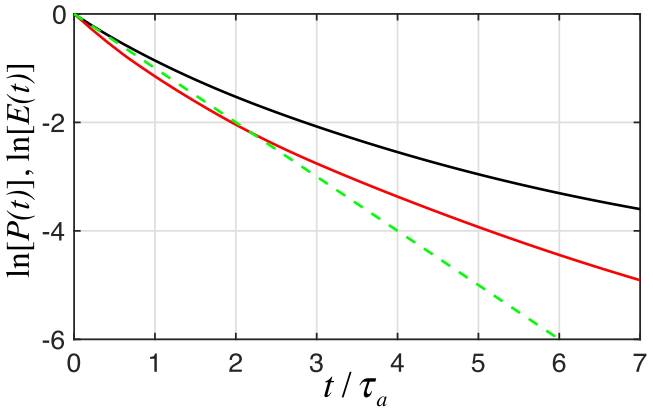

FIG. 4. Stored energy $E(t) = \hbar\omega_a \sum_M M\rho_M(t)$ (solid black line) and the radiated power $P(t) = -dE(t)/dt$ (solid red line) for a numerical simulation for the nominal conditions of our experiment: $N = 0.65$ million initially excited atoms (1.3 million atoms with an excitation fraction of 0.5) and a cloud radius of $R = 0.26$ mm. For comparison, the case of independent decay, $\exp(-t/\tau_a)$, is also plotted (dashed green line).

V. EXPERIMENTAL RESULTS

A. On-resonance versus detuned excitation

Figure 5 shows $\ln[(E(t)]$ for two different optical depths, OD = 1 (black line) and OD = 0.35 (blue line), contrasting on-resonance ($\Delta = 0$) versus detuned ($\Delta = 4.2\Gamma_a$) excitation. For both cases, the results are qualitatively similar with strong overall subradiance for OD = 1. This is consistent with the measurements of the Kaiser group (Refs. [8] and [9]), who also did not find much difference in the subradiance time scales between on-resonant versus detuned excitation and argued this to be a key indication of subradiance, rather than radiation trapping. Radiation trapping is critically important for atomic clouds with a very large on-resonant OD. It is less relevant in our experiment since the OD of the atomic cloud is of order unity or less. We will discuss the issue of radiation trapping in detail in Sec. VI below.

All of the data shown in the rest of the paper are taken at a detuning of $\Delta = 4.2\Gamma_a$.

B. Optical depth scan

Figure 6 shows $\ln[(E(t)]$ for an on-resonant optical depth of OD = 1, 0.83, 0.68, 0.52, and 0.35, respectively. The optical depth is varied by turning off the MOT beams and letting the cloud free expand for a certain duration of time before the excitation beam is applied. The five optical depths are obtained after an expansion time of 0, 1, 2, 3, and 4 ms, respectively. The optical depth after each expansion is calculated by measuring the size of the cloud using the EMCCD. As expected, as the optical depth is reduced, the subradiance is less pronounced and the decay rate approaches that of independent (i.e., uncorrelated) decay.

In each plot, the dashed red line is the result of the theoretical model with the free parameter adjusted to be $\xi = 0.77$. This parameter is adjusted once to get a good overall fit for $0 < t < 9\tau_a$ for the top plot (i.e., for OD = 1). There is no further adjustment for the consequent plots. With this single fitting parameter, there is good agreement between the experimental data and the numerical results. For comparison, the case of independent decay, $\exp(-t/\tau_a)$, is also plotted (dashed green line).

For the data of Fig. 6, the decay is not a simple exponential decay and as a result there is not a single time constant. In Fig. 7, we plot the mean decay time constant for each experimental curve shown in Fig. 6 during $0 < t < 2.3\tau_a$. The error bar in each data point is the standard variation of the decay time during this time window and is therefore a measure of how much the decay time changes during the same time window. The black curve is the result of numerical simulations where the free parameter is adjusted to get a good agreement for OD = 1 and $\xi = 0.94$. Again, with this single fitting parameter, there is good agreement between the experimental data and the numerical results. Consistent with the numerical results, there is some indication of a nonlinear dependence to the optical depth, since the data points do not lie on a single line and instead curve upwards as the OD is increased.

C. Excitation fraction scan

In Ref. [8], subradiance was studied in the weak excitation regime where the single-atom excited subspace is a good

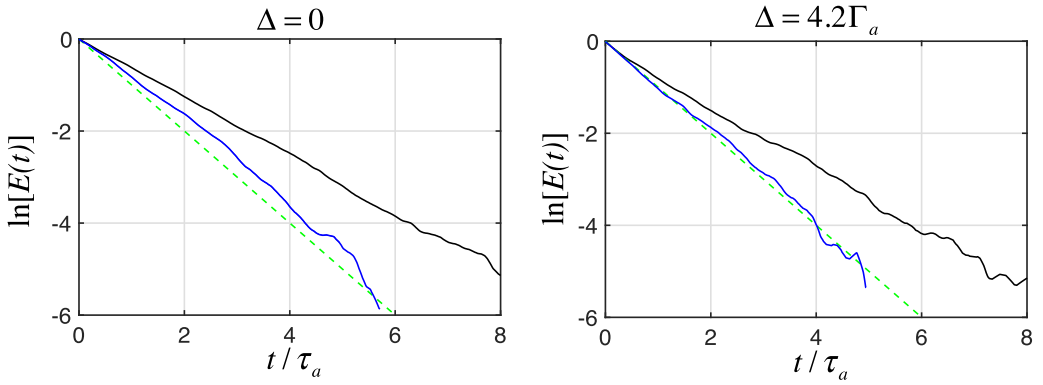

FIG. 5. Stored energy in the cloud (i.e., excited-state population) $\ln[(E(t)]$ for two different on-resonant optical depths, OD=1 (black line) and OD=0.35 (blue line). The plot on the left is obtained for an excitation laser which is on-resonant($\Delta = 0$), while for the plot on the right the excitation laser is detuned by an amount $\Delta = 4.2\Gamma_a$. For comparison, the case of independent decay, $\exp(-t/\tau_a)$, is also plotted (dashed green line). Because the results are qualitatively similar, the observed subradiance cannot be due to radiation trapping.

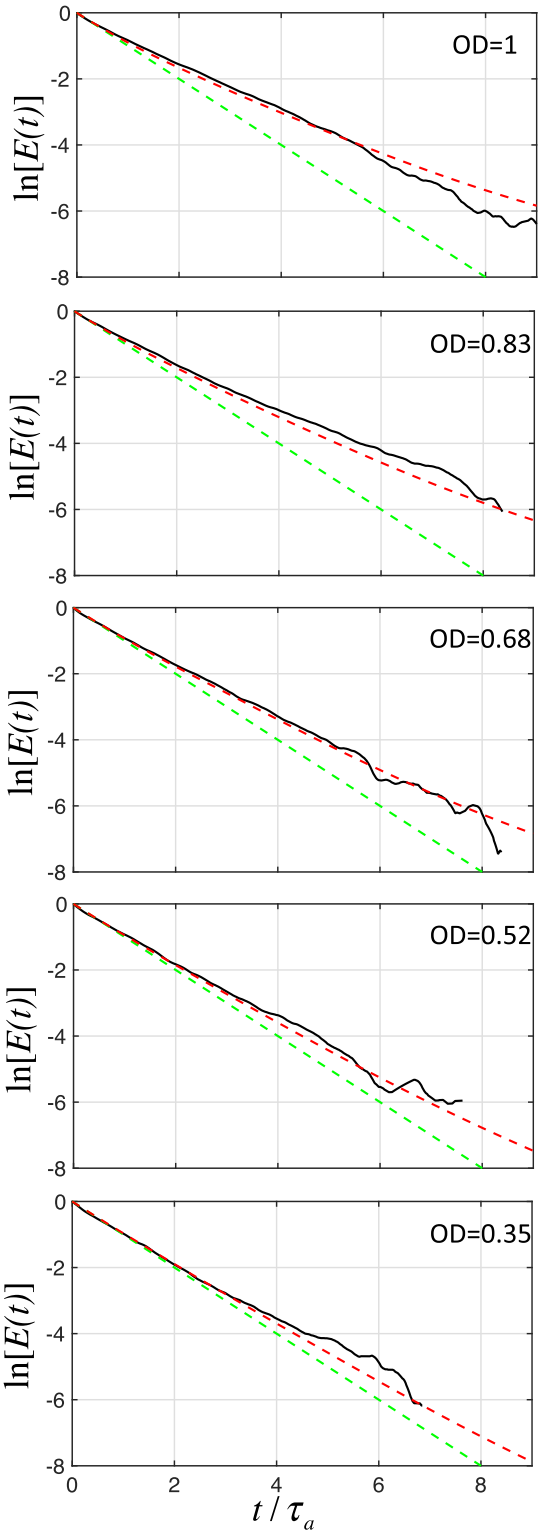

FIG. 6. $\ln[(E(t)]$ as the optical depth is varied from OD = 1 (top plot) to OD = 0.35 (bottom plot). In each plot, the dashed red line is the result of the theoretical model discussed in the text. For comparison, the case of independent decay, $\exp(-t/\tau_a)$, is also plotted (dashed green line). As expected, as the optical depth is reduced, the observed subradiance is reduced and the decay approaches independent (i.e., uncorrelated) decay. Only one value of ξ is used for all plots, demonstrating that the physical model can predict the dependence of collective effects on atomic density.

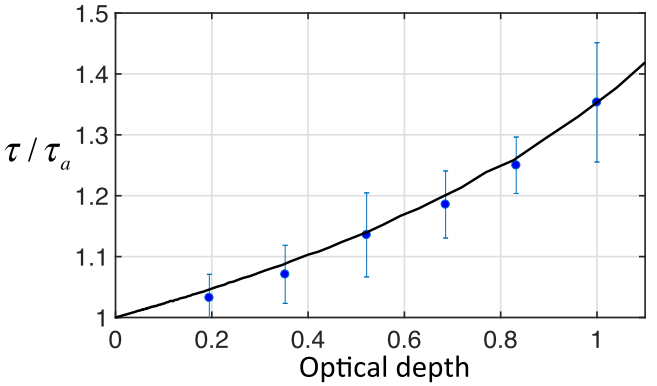

FIG. 7. Mean decay time for each experimental curve shown in Fig. 6 during $0 < t < 60$ ns. The error bar in each data point is the standard variation of the decay time during this time window and is therefore a measure of how much the decay time changes during the same time window.

approximation to the full dynamics. In this regime, the observed subradiant time scales are independent of the intensity of the excitation laser. In this section, we discuss that, in the dilute clouds and in the strong excitation regime, this is no longer the case. Figure 8 shows $\ln[(E(t)]$ for a high excitation fraction of 0.3 (solid black curve) and a relatively low excitation fraction of 0.08 (blue curve). For low excitation fraction, the decay approaches that of independent decay (dashed green line) and the observed subradiance is greatly reduced.

Figure 9 shows the mean decay time during $0 < t < 2.3\tau_a$ for 12 experimental curves similar to the ones shown in Fig. 8. While there is a large spread in the data, there is also a clear trend that, as the excitation fraction is increased, the decay time scales increase (i.e., the system becomes more subradiant). The solid black curve is the result of numerical results where the free parameter is adjusted to get a good agreement for the high excitation fraction of 0.3, $\xi = 0.90$. Again with this single fitting parameter, there is good agreement between the model and the experimental results.

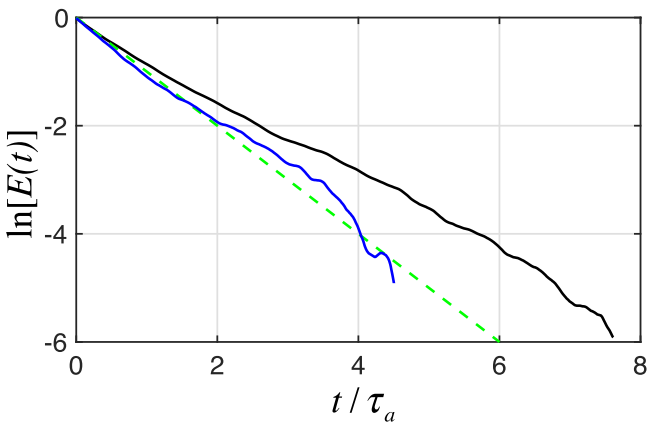

FIG. 8. $\ln[(E(t)]$ for high excitation fraction of 0.3 (solid black curve) and 0.08 (blue curve). For comparison, the case of independent decay, $\exp(-t/\tau_a)$, is also plotted (dashed green line). The amount of observed subradiance is significantly reduced as the excitation fraction is reduced.

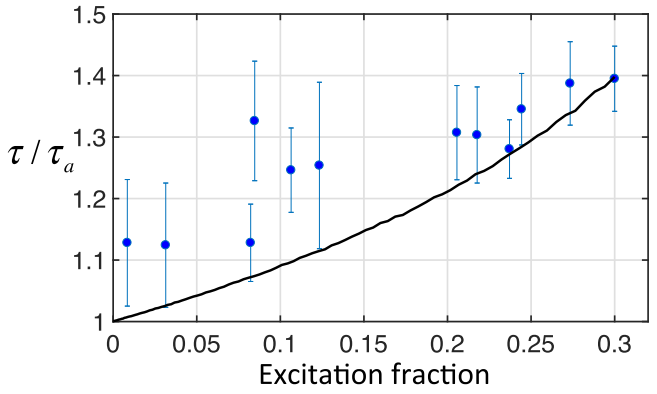

FIG. 9. Mean decay time during $0 < t < 2.3\tau_a$ as a function of the excitation fraction of the atomic cloud. The error bar in each data point is the standard variation of the decay time and is therefore a measure of how much the decay time changes during the same time window. The solid black curve is the result of numerical results with a single adjustable parameter. While there are large fluctuations in the data, the trend is clear; subradiant time scales increase with excitation fraction.

D. Signatures of superradiance-to-subradiance transition

In this section, we focus on the variation of the decay time as the system evolves—specifically on the superradiant-to-subradiant transition. For this purpose, we focus on the dynamics in the early times of the system evolution, $0 < t < 3\tau_a$. As shown in Fig. 2, while both curves, in principle, contain the same amount of information, the variation of the decay time constant during time evolution (i.e., how much each curve deviates from a linear line in the logarithmic plot) is more pronounced for the fluorescence curve. For this purpose, in this section we focus directly on the fluorescence as observed on the photon counter, $\ln[P(t)]$.

Figure 10 shows the observed fluorescence (solid blue lines) in logarithmic scale, $\ln[P(t)]$, for an on-resonant cloud optical depth of (a) OD = 1, (b) 0.83, (c) 0.68, and (d) 0.52. This data is obtained from the same data sets as the first four plots of Fig. 6. In these plots we focus on a shorter time window of $0 < t < 3\tau_a$ to focus on early stages of the decay. For comparison, the case of independent decay, $\exp(-t/\tau_a)$, is also plotted (dashed green line). For all the sets, there are signatures of faster than independent decay (superradiant) dynamics for $t < \tau_a$. For each set, the $\pm\sigma$ statistical error bars on the data points are also plotted (dotted blue lines) to demonstrate that the observed superradiance is well beyond the statistical error bars of the data. The error bars increase as the system evolves due to the reduced number of detected photons at later times of the decay. As the system evolves, superradiance either evolves to subradiance [high optical depth: (a) and (b)] or approaches independent decay [low optical depth: (c) and (d)].

Figure 11 shows the observed fluorescence for two optical depths OD = 1 (high) and OD = 0.52 (low) over a longer time window $0 < t < 7\tau_a$, and also overlapped with the numerical results (dashed red curves). Here, the free parameter is adjusted only once to be $\xi = 0.9$, in order to get good agreement with the experimental results for the high optical depth (left plot). For this case, the numerical results capture

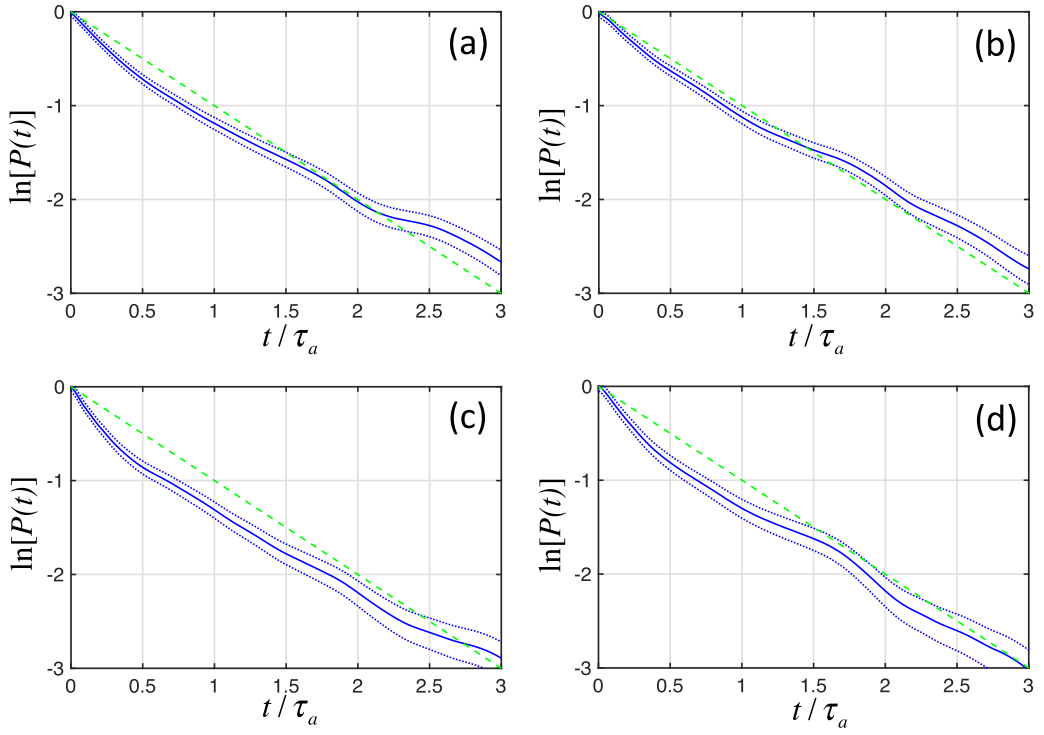

FIG. 10. Observed fluorescence (solid blue lines) in logarithmic scale for a cloud optical depth of (a) OD = 1, (b) 0.83, (c) 0.68, and (d) 0.52. For comparison, the case of independent decay, $\exp(-t/\tau_a)$, is also plotted (dashed green line). For each set, the $\pm\sigma$ statistical error bars on the data points are also plotted (dotted blue lines) to demonstrate that the observed superradiance is well beyond the error bars of the data. The error bars increase as the system evolves due to the reduced number of detected photons at later times of the decay.

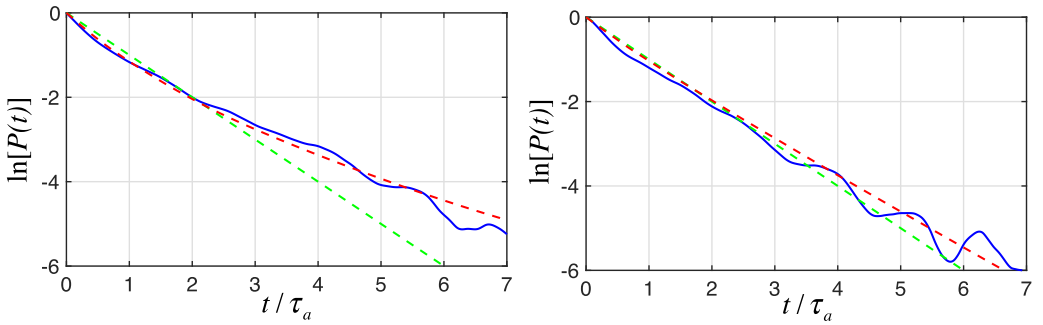

FIG. 11. Observed fluorescence in logarithmic scale for a cloud optical depth of OD = 1 (left) and 0.52 (right). For comparison, the numerical results are also plotted (dashed red curves).

the variation of the decay time constant during time evolution, as well as superradiance-to-subradiance transition very well. For the lower optical depth (right plot), the agreement between the experimental data and the numerical results is worse. Specifically, the experimental curve continues to show signatures of superradiance at early times, while the numerical results do not. The reason for this discrepancy is currently an open question. We speculate that one reason for the discrepancy could be the assumption of a uniform cloud in the numerical simulations. In the experiment, the density of the MOT is unlikely to be uniform, due to the complicated three-dimensional interference pattern produced by the six MOT laser beams. Due to this interference, there are likely localized regions with a higher density, which may be responsible for the persistent superradiant feature at early times, even at low optical depths.

VI. DISCUSSION: RADIATION TRAPPING VS SUBRADIANCE

It is well known that on-resonant radiation trapping, which is critically important for atomic clouds with a large optical depth, can mimic subradiance. Radiation trapping is a result of incoherent absorption and reemission of resonant photons in the atomic cloud, while subradiance is due to coherent antiphasing of the atomic dipoles. These two different physical effects can be distinguished even in atomic clouds with a very large optical depth [9]. In this section, we discuss a few important aspects of our experiment that indicate that radiation trapping does not play an important role. The first important point is that the on-resonant OD of the atomic cloud in our experiments is of order unity. We measure the optical depth using two different methods. In the first one, we measure the absorption of a weak resonant beam through the cloud. In the second approach, we monitor continuous fluorescence of the MOT atoms with the EMCCD under full saturation. Using the detected photon counts at the EMCCD and known solid angle of the collection optics, optical losses, and quantum efficiency of detection, we can then infer the number of atoms in the MOT. Together with the measurement of the size of the MOT cloud, this then allows us to infer the optical depth. We have found these two different measurements of the OD to be reasonably consistent, agreeing to within a factor of 2. We note that this estimation of the optical depth using the second approach is complicated by a number of issues, such as (i) the uncertainty in the number of atom measurement, (ii) the unknown distribution of the atoms among specific m_F sublevels in the $F = 2$ ground level, and (iii) the deviation of the shape of the atomic cloud from spherical. Because of these issues, the direct measurement of the optical depth using absorption of a weak probe laser beam is more reliable. As a result, in the above, we report the OD measurements using the absorption of a weak resonant beam.

For atomic clouds with near-uniform illumination, radiation trapping is predicted to be negligible at such low optical depths. For example, as discussed in Ref. [9], exact Monte Carlo simulations suggest that optical depths far larger than unity are needed for multiple scattering events (which result in radiation trapping) to become appreciable.

We also note that our experimental data of Fig. 9 largely rules out radiation trapping playing a dominant role. In this plot, we show that the subradiant time scales increase as the excitation fraction of the cloud (i.e., the initial number of atoms in the excited state) increases. If radiation trapping was playing a dominant role, one would expect exactly the opposite behavior: i.e., the subradiant time scales should have decreased as the excitation fraction is increased. This is because, for larger excitation fractions, there are fewer atoms in the cloud initially in the ground state and the probability of a photon being absorbed by the cloud decreases (i.e., the "effective" optical depth of the cloud is reduced as the excitation fraction is increased).

VII. CONCLUSIONS AND FUTURE WORK

In conclusion, we experimentally studied subradiance in a dilute cloud of ultracold ^{87}Rb atoms with densities very far away from the Dicke limit ($n\lambda_a^3 \sim 10^{-2}$) and where the on-resonance optical depth of the cloud is of order unity. Although collective decay is an old and well-studied problem, our results are unique in a number of ways. Perhaps most importantly, we were able to observe signatures of superradiant-to-subradiant transition; i.e., initially the decay rate is faster than independent decay (superradiant emission), while at later times it transitions to a slower rate (subradiant emission). Such a transition has long been predicted to be an important feature of collective decay, but has not been observed before. We also showed that, in the regime

that we study (dilute cloud in the strong excitation regime), the subradiant time scales depend on the excitation fraction of the cloud (i.e., on the intensity of the excitation pulse).

We also discussed a theoretical model whose results are in good agreement with the experiments. The model relies on extension of the well-known decay ladder of the excitation, where the decay rate of each subspace is modified in accordance with the eigenvalue distribution of the exchange Hamiltonian. The model captures the observed (i) variation of the decay time constant with optical depth, (ii) variation of the decay time constant with the excitation fraction, and (iii) the subradiant-to-superradiant transition. However, the model overestimates the variation of the decay time as the system evolves: the curves shown in Fig. 4 deviate more from linear compared to experimental curves. The model also does not capture the persistent superradiance at early times that we observe in the experiment, even at low optical depths.

Extension of our results to mesoscopic ultracold clouds, with atom numbers in the range of 100–1000, would be very interesting. Such a mesoscopic system can be studied by loading the atoms to a far-off-resonant dipole trap, which is formed by focusing a detuned laser overlapping with the MOT. By moving one of the mirrors of the focusing optics, the beam size at the focus, and therefore the size of the trap, can be precisely controlled. This would allow independent control of the number (N) and density (n) of atoms in the trap. Such highly controlled mesoscopic systems will likely allow for better probing of many of the physics that we have explored in this paper, including the superradiance-to-subradiance transition.

Our results have important implications for a number of research areas. Perhaps the most important immediate application is to quantum information science. As mentioned above, subradiant states have gained renewed attention over the past decade since they are less susceptible to decoherence. Our work experimentally shows that such states can, in principle, be prepared even in the large-sample, very dilute limit.

On a more fundamental note, Ref. [10] discussed the implications of cooperative effects for scalability of quantum computers. Specifically, it was shown that noise due to collective decay produced errors in a quantum computer beyond the applicability of the threshold theorem and therefore outside the current models of quantum error correction. The key reason for this is that cooperative effects cannot be ignored, even when the average distance between the qubits is larger than the emission wavelength. Our experiment indeed shows that this is the case: even when on average there is only 0.01 atoms in a cubic wavelength of volume, cooperative effects can be quite important.

ACKNOWLEDGMENTS

We thank D. Gold, J. Karpel, Z. Buckholtz, and S. Inbar for many helpful discussions. We also would like to thank J. Miles for his experimental contributions at the early stages of this project.

APPENDIX: DETAILS OF THE THEORETICAL MODEL AND NUMERICAL SIMULATIONS

1. Formalism and the exchange interaction

Consider N two-level atoms, each with levels $|0\rangle$ and $|1\rangle$, in a three-dimensional geometry. We denote each individual atom with the index j and consider a continuum of electromagnetic modes with annihilation and creation operators $\hat{a}_{\kappa\epsilon}$ and $\hat{a}^\dagger_{\kappa\epsilon}$, respectively. These operators act on the mode of the field with wave vector κ and polarization ϵ. The total Hamiltonian for the system when only the energy-conserving terms are retained (under the rotating wave approximation) is [10]

$$\begin{aligned}\hat{H}_{\text{total}} = &\sum_j \frac{1}{2}\hbar\omega_a\hat{\sigma}_z^j + \sum_{\kappa\epsilon}\hbar\nu_{\kappa\epsilon}\left(\hat{a}^\dagger_{\kappa\epsilon}\hat{a}_{\kappa\epsilon} + \frac{1}{2}\right)\\ &- \sum_j\sum_{\kappa\epsilon}\hbar g_{\kappa\epsilon}\big[\hat{a}_{k\epsilon}\exp(i\vec{\kappa}\cdot\vec{r}_j)\hat{\sigma}_+^j\\ &+ \hat{a}^\dagger_{\kappa\epsilon}\exp(-i\vec{\kappa}\cdot\vec{r}_j)\hat{\sigma}_-^j\big],\end{aligned} \tag{A1}$$

where

$$\begin{aligned}\hat{\sigma}_z^j &= |1\rangle^j{}^j\langle 1| - |0\rangle^j{}^j\langle 0|,\\ \hat{\sigma}_+^j &= |1\rangle^j{}^j\langle 0|,\\ \hat{\sigma}_-^j &= |0\rangle^j{}^j\langle 1|.\end{aligned} \tag{A2}$$

In Eq. (A1), the first two terms describe the atoms and the electromagnetic modes in the absence of any interaction, whereas the third term describes the coupling between the two systems. $\vec{r}_j$ is the position of the jth atom and the energies of the atom states $|0\rangle$ and $|1\rangle$ are taken to be $-\frac{1}{2}\hbar\omega_a$ and $\frac{1}{2}\hbar\omega_a$, respectively. The Dicke limit of the above equations is obtained when the total size of the sample is assumed to be small compared to the κ vector of the relevant modes, i.e., $\vec{\kappa}\cdot\vec{r}_j \to 0$.

It is now well understood that the key physical effect that describes many different aspects of collective decay, including superradiance and subradiance, is the exchange interaction. Starting with the Hamiltonian of Eq. (A1), this interaction has been derived using a variety of approaches by a number of authors [5,57–59]. One such derivation of the exchange interaction Hamiltonian is given in our earlier paper, Ref. [10], which we summarize here. The derivation uses assumptions that are similar to the traditional Wigner-Weisskopf theory of spontaneous decay [60]. Briefly, we take the initial atomic system to be an arbitrary superposition (in general entangled state) and assume initially zero excitation in each electromagnetic mode $\kappa\epsilon$. We then study the problem in the interaction picture and integrate out the probability amplitudes of the continuum states using the usual Born-Markov approximation. Using this approach, the end result is the following effective interaction Hamiltonian:

$$\hat{H}_{\text{eff}} = \sum_j\sum_k \hat{H}^{jk}. \tag{A3}$$

Here, the sum is over all pairs of qubits and operators $\hat{H}^{jk}$ act nontrivially only on the qubits with indices j and k,

$$\hat{H}^{jk} = F_{jk}\hat{\sigma}_+^j\hat{\sigma}_-^k + F_{kj}\hat{\sigma}_-^i\hat{\sigma}_+^j, \tag{A4}$$

which is essentially a "spin" exchange interaction (mediated by photon modes) with coupling constants of F_{jk}:

$$F_{jk} = F_{kj} = -\left(i\frac{\Gamma_a}{2} + \delta\omega_a\right)\frac{3}{2}\left[(1-\cos^2\theta_{jk})\frac{\sin\kappa_a r_{jk}}{\kappa_a r_{jk}} + (1-3\cos^2\theta_{jk})\left(\frac{\cos\kappa_a r_{jk}}{(\kappa_a r_{jk})^2} - \frac{\sin\kappa_a r_{jk}}{(\kappa_a r_{jk})^3}\right)\right]. \tag{A5}$$

Here, Γ_a is the single-atom decay rate and $\delta\omega_a$ is the single-atom Lamb shift of the qubit transition. r_{jk} is the distance between the two atoms and θ_{jk} is the angle between the atomic dipole moment vector and the separation vector $\vec{r}_{jk}$. The quantity κ_a is the wave vector for the electromagnetic modes energy resonant with the qubit transition: $\kappa_a = \omega_a/c$.

2. Width of the eigenvalue distribution for M subspace

In this section, we discuss the width of the eigenvalue spectrum of the exchange Hamiltonian $\hat{H}_{\text{eff}} = \sum_{jk}\hat{H}^{jk} = \sum_k F_{jk}\hat{\sigma}_+^j\hat{\sigma}_-^k + F_{kj}\hat{\sigma}_-^j\hat{\sigma}_+^k$ in the $N\to\infty$ limit, for the M-atom excited subspace. In this limit, the eigenvalues λ of $\hat{H}_{\text{eff}}$ can be viewed as having a continuous distribution with probability density function $f_\Lambda(\lambda) \equiv P\{\Lambda = \lambda\}$. The width of the probability density function can be evaluated by explicitly calculating the second moment (variance) of the distribution $\sigma^{(2)} \equiv E[\Lambda^2] = \int f_\Lambda(\lambda)\lambda^2 d\lambda$, where $E[\ldots]$ stands for the expected value. By definition, this second moment is

$$\sigma^{(2)} = E[\Lambda^2] = \binom{N}{M}^{-1}\text{Trace}[(\hat{H}_{\text{eff}})^2] = \binom{N}{M}^{-1}\sum_q\langle q|\left(\sum_{jk}F_{jk}\hat{\sigma}_+^j\hat{\sigma}_-^k + F_{kj}\hat{\sigma}_-^j\hat{\sigma}_+^k\right)^2|q\rangle. \tag{A6}$$

Here, the summation q is over all the states in the M atom excited subspace. By inspection, each term $\langle q|(\sum_{jk}F_{jk}\hat{\sigma}_+^j\hat{\sigma}_-^k + F_{kj}\hat{\sigma}_-^j\hat{\sigma}_+^k)^2|q\rangle$ produces $(N-M)M$ contributions, each appropriately scaled with the square of the relevant coupling constant, F_{jk}^2. In the $N\to\infty$ limit, the result is therefore

$$\sigma^{(2)} = (N-M)ME\left[F_{jk}^2\right] = \frac{\pi + 29/12}{k_a^2R^2}(N-M)M\Gamma_a^2. \tag{A7}$$

Here, in the last step, we have used the expected value of the squares of the coupling constants in a three-dimensional geometry, $E[F_{jk}^2]$, as discussed in Ref. [10]. The standard deviation (width) of the distribution is the square root of the variance given in Eq. (A7):

$$\sigma = \sqrt{\sigma^{(2)}} = \frac{\sqrt{\pi + 29/12}}{k_aR}\sqrt{N-M}\sqrt{M}\Gamma_a. \tag{A8}$$

The distribution is symmetric around $\lambda = 0$, which means that there are an equal number of superradiant and subradiant states. We have numerically checked that the results are insensitive to the precise shape of the distribution; rather, as expected, the width is critical. As a result, we choose a simple uniform distribution centered around $\lambda = 0$, with a width given by Eq. (A8).

3. Heuristic incorporation of stimulated emission

The formalism described above assumes each photon mode to be unoccupied initially and, as a result, it does not incorporate stimulated emission in the decay process. In the small sample regime, an M-atom subspace has "M" photons stored and the spontaneous rates would at most be enhanced by "M," as the system decays through the ladder. This is because the stimulated emission rate for an M-photon state is a factor of M larger than the spontaneous rate [60]. For a large sample, all emitted photons would not interfere constructively, but instead interfere with random phases. As a result, we hypothesize that one would expect $\sqrt{M}$ enhancement compared to the spontaneous rate for the large sample. We, therefore, multiply the width given by Eq. (A8) by a factor of $\sqrt{M}$ to heuristically incorporate for stimulated emission.

[1] R. H. Dicke, Coherence in spontaneous radiation processes, Phys. Rev. **93**, 99 (1954).

[2] M. Gross and S. Haroche, Superradiance: An essay on the theory of collective spontaneous emission, Phys. Rep. **93**, 301 (1982).

[3] E. Wolfe and S. F. Yelin, Certifying Separability in Symmetric Mixed States of N Qubits, and Superradiance, Phys. Rev. Lett. **112**, 140402 (2014).

[4] R. T. Sutherland and F. Robicheaux, Coherent forward broadening in cold atom clouds, Phys. Rev. A **93**, 023407 (2016).

[5] I. E. Mazets and G. Kurizki, Multi-atom cooperative emission following single photon absorption: Dicke-state dynamics, J. Phys. B: At., Mol., Opt. Phys. **40**, F105 (2007).

[6] N. Skribanowitz, I. P. Herman, J. C. MacGillivray, and M. S. Feld, Observation of Dicke Superradiance in Optically Pumped HF Gas, Phys. Rev. Lett. **30**, 309 (1973).

[7] R. Friedberg, S. R. Hartmann, and J. T. Manassah, Frequency shifts in emission and absorption by resonant systems of two-level atoms, Phys. Rep. **7**, 101 (1973).

[8] W. Guerin, M. O. Araujo, and R. Kaiser, Subradiance in a Large Cloud of Cold Atoms, Phys. Rev. Lett. **116**, 083601 (2016).

[9] P. Weiss, M. O Araújo, R. Kaiser, and W. Guerin, Subradiance and radiation trapping in cold atoms, New J. Phys. **20**, 063024 (2018).

[10] B. Lemberger and D. D. Yavuz, Effect of correlated decay on fault-tolerant quantum computation, Phys. Rev. A **96**, 062337 (2016).

[11] B. McGuyer *et al.*, Precise study of asymptotic physics with subradiant ultracold molecules, Nat. Phys. **11**, 32 (2015).

[12] R. G. DeVoe and R. G. Brewer, Observation of Superradiant and Subradiant Spontaneous Emission of Two Trapped Ions, Phys. Rev. Lett. **76**, 2049 (1996).

[13] D. Pavolini, A. Crubellier, P. Pillet, L. Cabaret, and S. Liberman, Experimental Evidence for Subradiance, Phys. Rev. Lett. **54**, 1917 (1985).

[14] P. Solano *et al.*, Super-radiance reveals infinite-range dipole interactions through a nanofiber, Nat. Commun. **8**, 1857 (2017).

[15] S. D. Jenkins, J. Ruostekoski, N. Papasimakis, S. Savo, and N. I. Zheludev, Many-Body Subradiant Excitations in Metamaterial Arrays: Experiment and Theory, Phys. Rev. Lett. **119**, 053901 (2017).

[16] P. Wolf, S. C. Schuster, D. Schmidt, S. Slama, and C. Zimmermann, Observation of Subradiant Atomic Momentum States with Bose-Einstein Condensates in a Recoil Resolving Optical Ring Resonator, Phys. Rev. Lett. **121**, 173602 (2018).

[17] S. J. Roof, K. J. Kemp, M. D. Havey, and I. M. Sokolov, Observation of Single-Photon Superradiance and the Cooperative Lamb Shift in an Extended Sample of Cold Atoms, Phys. Rev. Lett. **117**, 073003 (2016).

[18] S. L. Bromley *et al.*, Collective atomic scattering and motional effects in a dense coherent medium, Nat. Commun. **7**, 11039 (2016).

[19] C. Bradac *et al.*, Room-temperature spontaneous superradiance from single diamond nanocrystals, Nat. Commun. **8**, 1205 (2017).

[20] A. Angerer *et al.*, Superradiant emission from color centres in diamond, Nat. Phys. **14**, 1168 (2018).

[21] Z. Wang *et al.*, Controllable Switching Between Superradiant and Subradiant States in a 10-qubit Superconducting Circuit, Phys. Rev. Lett. **124**, 013601 (2020).

[22] M. O. Scully and A. A. Svdzinsky, The super of superradiance, Science **325**, 1510 (2009).

[23] M. O. Scully, E. S. Fry, C. H. Raymond Ooi, and K. Wódkiewicz, Directed Spontaneous Emission from an Extended Ensemble of *N* Atoms: Timing Is Everything, Phys. Rev. Lett. **96**, 010501 (2006).

[24] E. Akkermans, A. Gero, and R. Kaiser, Photon Localization and Dicke Superradiance in Atomic Gases, Phys. Rev. Lett. **101**, 103602 (2008).

[25] A. A. Svidzinsky, J.-T. Chang, and M. O. Scully, Cooperative spontaneous emission of *N* atoms: Many-body eigenstates, the effect of virtual Lamb shift processes, and analogy with radiation of *N* classical oscillators, Phys. Rev. A **81**, 053821 (2010).

[26] A. A. Svidzinsky and J.-T. Chang, Cooperative spontaneous emission as a many-body eigenvalue problem, Phys. Rev. A **77**, 043833 (2008).

[27] H. Cai, D.-W. Wang, A. A. Svidzinsky, S.-Y. Zhu, and M. O. Scully, Symmetry protected single photon subradiance, Phys. Rev. A **93**, 053804 (2016).

[28] P. A. Vetter *et al.*, Single photon subradiance and superradiance revisited: a group theoretic analysis of subradiant states, Phys. Scr. **91**, 023007 (2016).

[29] F. Cottier, R. Kaiser, and R. Bachelard, Role of disorder in super- and subradiance of cold atomic clouds, Phys. Rev. A **98**, 013622 (2018).

[30] M. O. Araújo, W. Guerin, and R. Kaiser, Decay dynamics in the coupled-dipole model, J. Mod. Opt. **65**, 1345 (2018).

[31] W. Guerin, M. T. Rouabah, and R. Kaiser, Light interacting with atomic ensembles: Collective, cooperative and mesoscopic effects, J. Mod. Opt. **64**, 895 (2017).

[32] W. Guerin and R. Kaiser, Population of collective modes in light scattering by many atoms, Phys. Rev. A **95**, 053865 (2017).

[33] T. Bienaimé, M. Petruzzo, D. Bigerni, N. Piovella, and R. Kaiser, Atom and photon measurement in cooperative scattering by cold atoms, J. Mod. Opt. **58**, 1942 (2011).

[34] J. H. Eberly, Emission of one photon in an electric dipole transition of one among N atoms, J. Phys. B **39**, S599 (2006).

[35] T. Bienaimé, N. Piovella, and R. Kaiser, Controlled Dicke Subradiance from a Large Cloud of Two-Level Systems, Phys. Rev. Lett. **108**, 123602 (2012).

[36] M. O. Scully, Collective Lamb Shift in Single Photon Dicke Superradiance, Phys. Rev. Lett. **102**, 143601 (2009).

[37] M. O. Scully, Single Photon Subradiance: Quantum Control of Spontaneous Emission and Ultrafast Readout, Phys. Rev. Lett. **115**, 243602 (2015).

[38] A. A. Kalachev and V. V. Samartsev, Quantum memory and quantum computations in the optical subradiance regime, Quantum Electron. **35**, 679 (2005).

[39] V. V. Temnov and U. Woggon, Superradiance and Subradiance in an Inhomogeneously Broadened Ensemble of Two-Level Systems Coupled to a Low-Q Cavity, Phys. Rev. Lett. **95**, 243602 (2005).

[40] P.-O. Guimond, A. Grankin, D. V. Vasilyev, B. Vermersch, and P. Zoller, Subradiant Bell States in Distant Atomic Arrays, Phys. Rev. Lett. **122**, 093601 (2019).

[41] A. Asenjo-Garcia, M. Moreno-Cardoner, A. Albrecht, H. J. Kimble, and D. E. Chang, Exponential Improvement in Photon Storage Fidelities Using Subradiance and "Selective Radiance" in Atomic Arrays, Phys. Rev. X **7**, 031024 (2017).

[42] S. D. Jenkins and J. Ruostekoski, Controlled manipulation of light by cooperative response of atoms in an optical lattice, Phys. Rev. A **86**, 031602 (2012).

[43] D. Plankensteiner, L. Ostermann, H. Ritsch, and C. Genes, Selective protected state preparation of coupled dissipative quantum emitters, Sci. Rep. **5**, 16231 (2015).

[44] R. J. Bettles, S. A. Gardiner, and C. S. Adams, Cooperative ordering in lattices of interacting two-level dipoles, Phys. Rev. A **92**, 063822 (2015).

[45] R. J. Bettles, S. A. Gardiner, and C. S. Adams, Cooperative eigenmodes and scattering in one-dimensional atomic arrays, Phys. Rev. A **94**, 043844 (2016).

[46] G. Facchinetti, S. D. Jenkins, and J. Ruostekoski, Storing Light with Subradiant Correlations in Arrays of Atoms, Phys. Rev. Lett. **117**, 243601 (2016).

[47] H. Zoubi and H. Ritsch, Metastability and directional emission characteristics of excitons in 1D optical lattices, Europhys. Lett. **90**, 23001 (2010).

[48] H. Zoubi and H. Ritsch, Lifetime and emission characteristics of collective electronic excitations in two-dimensional optical lattices, Phys. Rev. A **83**, 063831 (2011).

[49] D. F. Kornovan, A. S. Sheremet, and M. I. Petrov, Collective polaritonic modes in an array of two-level quantum emitters coupled to an optical nanofiber, Phys. Rev. B **94**, 245416 (2016).

[50] S. Prasad and R. J. Glauber, Polarium model: Coherent radiation by a resonant medium, Phys. Rev. A **61**, 063814 (2000).

[51] D. Bhatti, R. Schneider, S. Oppel, and J. von Zanthier, Directional Dicke Subradiance with Nonclassical and Classical Light Sources, Phys. Rev. Lett. **120**, 113603 (2018).

[52] R. Wiegner, J. von Zanthier, and G. S. Agarwal, Quantum-interference-initiated superradiant and subradiant emission from entangled atoms, Phys. Rev. A **84**, 023805 (2011).

[53] C. E. Máximo, R. Bachelard, F. E. A. dos Santos, and C. J. Villas-Boas, Cooperative spontaneous emission via renormalization approach: Classical versus semi-classical effects, Phys. Rev. A **101**, 023829 (2020).

[54] N. A. Proite, Z. J. Simmons, and D. D. Yavuz, Observation of atomic localization using electromagnetically induced transparency, Phys. Rev. A **83**, 041803(R) (2011).

[55] J. A. Miles, Z. J. Simmons, and D. D. Yavuz, Subwavelength Localization of Atomic Excitation Using Electromagnetically Induced Transparency, Phys. Rev. X **3**, 031014 (2013).

[56] B. E. Unks, N. A. Proite, and D. D. Yavuz, Generation of high-power laser light with GHz splitting, Rev. Sci. Instrum. **78**, 083108 (2007).

[57] S. Utsunomiya, C. P. Master, and Y. Yamamoto, Algorithm-based analysis of collective decoherence in quantum computation, J. Opt. Soc. Am. B **24**, 198 (2007).

[58] I. M. Sokolov, M. D. Kupriyanova, D. V. Kupriyanov, and M. D. Havey, Light scattering from a dense and ultracold atomic gas, Phys. Rev. A **79**, 053405 (2009).

[59] L. H. Pedersen and K. Molmer, Few qubit atom-light interfaces with collective encoding, Phys. Rev. A **79**, 012320 (2009).

[60] Y. Yamamoto and A. Imamoglu, *Mesoscopic Quantum Optics* (John Wiley & Sons, New York, 1999).